Title:

Alkali elution behavior of steelmaking slag packed in an open channel vessel in seawater

Authors:

Yamato MATSUDA[1)], Md. Azhar UDDIN[1)], Yoshiei KATO[1)], Yasuhito MIYATA[2)], Eiji KISO[3)]

1) Department of Material and Energy Science, Graduate School of Environmental and Life Science, Okayama University, 1-1 Tsushima-naka, 3-chome, Kita-ku, Okayama,700-8530 Japan

2) Slag & Refractories Research Department, Steel Research Laboratory, JFE Steel Corporation

3) Marketing Development, Slag & Cement Division, Nippon Steel Corporation

E-mail address:

Yamato MATSUDA[1)]: pid86xq4@s.okayama-u.ac.jp

1 Md. Azhar UDDIN[1)]: alazhar@cc.okayama-u.ac.jp

2 Yoshiei KATO[1)] : y-kato@cc.okayama-u.ac.jp （Corresponding author）

3 Yasuhito MIYATA[2)]: y-miyata@jfe-steel.co.jp

4 Eiji KISO[3)]: kiso.664.eiji@jp.nssmc.com

5

6

1 Abstract:

2 The alkali elution behavior of steelmaking slag in seawater was kinetically investigated and
3 simulated under continuous flow in an open channel vessel with packed bed of steelmaking slag.
4 Two types of steelmaking slags, viz. decarburization slag and dephosphorization slag, were used
5 in this study. The alkali elution rate of decarburization slag was larger than that of
6 dephosphorization slag due to larger free CaO content. The pH value for dephosphorization slag
7 was almost the same as the seawater pH value in 3-4 days, whereas that for decarburization slag
8 was stabilized in 3 days although the pH value was slightly larger than that of seawater. The
9 capacity coefficients of alkali elution for dephosphorization and decarburization slags decreased
10 together in an exponential manner with time. Based on a regression equation on the mass
11 transfer capacity coefficient change with time, the alkali elution behavior was simulated and the
12 calculated results agreed well with experimental ones. The temporal pH change was predicted
13 by changing slag surface area and seawater flow rate as a parameter. According to the
14 simulation results for dephosphorization slag, the seawater pH value did not reach a high level
15 in the ocean area.

16

17 Key words: steelmaking slag, alkali elution, seawater, open channel, packed bed

"Main text"

1. Introduction

Steelmaking slag has been utilized in ocean area as sea-grass beds due to its rich source of minerals such as iron oxide and silicon oxide [1-11], a usable material to prevent seawater contamination caused by sulfide contained in the bottom soil matter of the sea [12-15], and materials to increase soil strength by mixing with dredged soil or bottom materials of the sea [16, 17]. However, a part of CaO in steelmaking slag exists as isolated free CaO and is decomposed into Ca^{2+} and OH^- ions in seawater. The seawater in the vicinity of area where steelmaking slag exists is alkalized in the early times despite a buffer effect of seawater [18-20]. While having higher pH value, $Mg(OH)_2$ is generated by the reaction of Mg^{2+} in seawater with OH^- from free CaO due to buffering action of Mg^{2+} to inhibit the increase in pH value. The surrounding seawater might become emulsified due to precipitated $Mg(OH)_2$, which is one of reasons to prevent the utilization of steelmaking slag in the ocean from prevailing widely in Japan. Thus, a scheme to examine pH increase in seawater due to steelmaking slag products was proposed and reported [21, 22].

On the other hand, basic studies on the alkali elution behavior of steelmaking slag into seawater have been reported. Tamaki et al. [23] indicated the effects of impeller rotation speed,

slag layer depth, slag/seawater ratio, free CaO content in slag, etc. on the alkali elution rate by a batch reactor experiment. Takeuchi et al. [24] examined the relationship between the alkali elution rate and process parameters such as seawater velocity, slag layer depth, slag diameter etc. and integrated it into a non-dimensional equation by a continuous stirred tank reactor experiment. Furthermore, Takeuchi et al. [25] found that the alkali elution rate became different from the non-dimensional equation when slag layer was larger and slag diameter was smaller by using two kinds of open channel apparatus. In their researches, slag was filled in a slag box just below the open channel bottom as schematically shown in Fig. 1 (a). The study was carried out to simulate the alkali elution caused by steelmaking slag piled on the ocean bed. However, these works [24, 25] reported the short-term alkali elution behavior until 60-120 min. Miyazaki et al. [26] and Kanayama et al. [27] also investigated the short period of alkali elution behavior in the open channel experiments.

As for the long-term alkali elution behavior, Kanayama et al. [28] combined the pH measurement in the real ocean area and theoretical analysis. Matsuda et al. [29] used the same open channel as Takeuchi et al. [25] and not only kinetically analyzed the alkali elution rate but also explained the decreasing mechanism of the alkali elution from slag into seawater through 1056 h of measurement. However, the alkali elution rate was insufficiently examined under the

conditions that seawater mainly flows between slag particles as schematically shown in Fig. 1 (b). For example, this situation occurs when slags are piled on the shallow place of a seacoast.

In this study, when seawater passed through the interval between slag particles packed in an open channel vessel (Fig. 1 (b)), the effects of the type of slag and slag diameter at the same surface area on pH change were investigated for 6 – 7 days. The alkali elution behavior was compared between decarburization slag with higher free CaO content and dephosphorization slag with lower free CaO content. Finally, the alkali elution model was proposed and the effects of operation factors were simulated on the basis of these results.

2. Experiment

2.1 Experimental method and conditions

A schematic diagram of open channel vessel, packed slag position and seawater sampling sites is shown in Fig. 2. Here, the seawater sampling sites were indicated in a, A, B, and C. The vessel was made of acrylic resin with 1.00 m in length, 0.12 m in width and 0.30 m in height. In order to keep the seawater flow uniform in the vessel, three and two current plates with a number of holes were installed on the up-stream and down-stream sides, respectively. Fresh

seawater at Ushimado-cho, Setouchi city, Okayama, Japan was used for the experiment. Although there is a possibility that the seawater pH may change depending on weather and season, sand filtration was only performed without adjusting the seawater content. The seawater flow rate was kept 3.61×10^{-4} m^3/s by installing an overflowing vessel at a given position higher than the open channel vessel. The calculated seawater velocity with no slag particles in the vessel was 0.020 m/s within the velocity near the sea floor [30].

The experiment began after the slag was charged until 0.10 m in height between the upstream and downstream current plates with fresh seawater flowing in the open channel. The seawater level in the open channel vessel was kept 0.15 m. As shown in Fig. 2, the origin was defined as the point of the vessel bottom located 0.235 m downstream from the upstream current plate and the width center. The flow direction, width, and height were indicated as x, y and z axes, respectively.

A schematic diagram of sampling positions for measuring seawater velocity and pH is shown in Fig. 3 The seawater pH was measured at the point a (-0.40, 0.0, 0.02), the seawater velocity and pH at the positions in line of A (-0.10, 0.0, z) and B (0.20, 0.0, z) between slag particles, and at the position in line of C (0.35, 0, z) surrounded by the two downstream current plates. Here, z values of A (-0.10, 0.0, z), B (0.20, 0.0, z) and C (0.35, 0, z) were 0.02, 0.05, 0.07,

1 0.10 and 0.13 m. About 5 mL of seawater was sucked up by a syringe connected with a
2 wire-supported silicon tube (0.8 mm in I. D. x 1.6 mm in O. D) at each position of A, B and C
3 and a given sampling time. A pH meter (Toa DK Co., LTD., MM60-R) was used for the pH
4 measurement and x-direction velocity was measured by electromagnetic flow meter (KENEK
5 Co., LTD, VM-1001).

6

7 2.2 Slag samples

8 The appearance of slag samples used for the experiment is shown in Fig. 4. The
9 dephosphorization slag of Slag I and II indicated the sponge-like body, whereas the
10 decarburization slag of Slag III and IV had the body similar to the angular solid stone.

11 Table 1 shows the slag features used for the experiment. As Slag I and III had smaller mean
12 diameter than Slag II and IV, Al_2O_3 balls (density: 3.6×10^3 kg/m^3) (AS ONE, Corp., HD-10,
13 HD-15) of 0.015 m in diameter were partly added so as to equalize the slag layer thickness and
14 surface area. The apparent density, ρ (kg/m^3), of decarburization slag (Slag III and IV) was
15 obtained by dividing slag mass by the increase in liquid volume during a group of slags
16 sedimentation in a measuring cylinder. On the other hand, assuming that the seawater inside

open small holes of sponge-like dephosphorization slag remains there and is not exchanged with the external seawater, the ρ value of dephosphorization slag was calculated from (Mass of Slag II used for the experiment) / (ρ of Slag II) = (Mass of Slag IV used for the experiment) / (ρ of Slag IV), which means the open holes in dephosphorization slag were filled with fictional weightless material. Slag I and III had a particle size range of 0.0095-0.0132 m, and Slag II and IV had that of 0.0132-0.0265 m. Assuming that the slag was spherical, the mean slag diameter, $<d>$ (m), was calculated from Eq. (1) by collecting some slag samples randomly and measuring mass, w (kg), and number, N (-).

$$<d> = \{6w/(\rho\pi N)\}^{1/3} \quad (1)$$

As the substitution of $<d>$, ρ and w into Eq. (1), led to the calculation of the number, N, of slag particles, the slag surface area, a_i (m^2), in this study was obtained from Eq. (2).

$$a_i = \pi<d>^2 N \quad (2)$$

Finally, the slag surface areas for dephosphorization slag (Slag I and II) and decarburization slag (Slag III and IV) were given by 1.08 and 1.07 m^2, respectively. The slag packing ratio was calculated between 52.3 – 56.0 %.

The chemical compositions of dephosphorization slag (Slag I and II) and decarburization

slag (Slag III and IV) are shown in Table 2. The main factor of alkali elution to the seawater is the dissolution of free CaO (f. CaO) from the slag surface. As indicated by Tamaki et al. [23], f. CaO exposure to the seawater increases with its increasing content in the slag even if the slag surface area is equal. Free CaO (f.CaO) content of decarburization slag was 3.29 mass %, whereas that of dephosphorization slag 0.08 mass %. The appearance of slag as shown in Fig. 4 suggested that the dephosphorization slag was a little bit more porous than decarburization slag.

3. Results and discussion

3.1 Seawater velocity profile in open channel vessel with packed bed of slag

The seawater velocity at A, B and C in the open channel vessel are shown in Figs.5 and 6 for decarburization slag with 9.5-13.2 mm and 13.2-26.5 mm in diameter, respectively. The alumina balls for the slag with 9.5-13.2 mm in diameter were blended so as to keep the same surface areas as the slag with 13.2-26.5 mm in diameter. The packed ratio of slag was 53.2 % for Fig. 5 and 52.4 % for Fig. 6 as shown in Table 1. The seawater flow rate was kept 1.30m^3/h. In this case, the seawater velocity, <u> (m/s), in uniform flow became 0.02 m/s without packed layer of slag. From both figures, the seawater velocity of the gap between slag particles became a small

value compared with that of the upper point without slag. The smaller the slag particle size was, the smaller the seawater velocity became at the slag-packed region of B and C. That is because the smaller slag particle size increased the water pressure imposed at the gap between slag particles which is more difficult to flow.

3.2 Temporal change of pH in open channel vessel

As shown in Fig. 3, the pH value at the point a(x, y, z) = a (-0.40, 0, 0.02) does not affect the alkali elution from slag and always indicates the seawater pH. It was almost constant from the beginning to the end of each experiment in this study.

The temporal changes of pH at each position in the open channel vessel are shown in Figs. 7 to 10 for Slag I to IV, respectively. The seawater pH value in Figs. 6 and 7 was 7.9, whereas that in Figs. 8 and 9 was 8.19. This difference depends on the pH variation in the season of seawater recognized in Seto Inland Sea [31] because the experiments were carried out throughout more than one season. Compared with the seawater pH, the pH values at A located upstream in the packed bed of slag was relatively small, those at B placed downstream was increased due to the accumulated alkali elution. As the seawater above and through the packed layer of slag joined

1 together at C, the pH value was smaller than that at B. The pH at close to the vessel bottom
2 indicated the higher value at any positions of A, B and C in line in Figs. 7-10. It is considered
3 that the lower seawater velocity near the bottom as seen in Figs 5 and 6 prolonged the
4 slag-seawater contact time.

5 The pH value of decarburization slag (Figs. 9 and 10) became larger than that of
6 dephosphorization slag (Figs. 7 and 8) at any positions in line of A, B and C. This is due to the
7 amount of free CaO on the slag surface which dissolves to the seawater by the reaction of CaO
8 + $H_2O \rightarrow Ca^{2+} + OH^-$. The higher free CaO content in the slag results to the larger alkali
9 elution rate. As shown in Figs. 9 and 10, it can be seen that the pH values of decarburization
10 slag near the vessel bottom was higher than that of seawater even during 6-7 days of the
11 experimental period, which means the CaO dissolution from the slag surface continued.

12 No difference of the temporal change in pH between the dephosphorization slag of Slag I
13 and II was recognized at A and B, and the pH value of Slag I was slightly higher than that of
14 Slag II at C. On the other hand, the decarburization slag of Slag III with smaller size indicated
15 approximately the same tendency of the temporal pH change as that of Slag IV with larger size
16 except the pH of B and C near the vessel bottom. On the basis of these results, it was known
17 that the equal slag surface area for the different size with the same kind (decarburization or

dephosphorization) leads to the same alkali elution rate.

3.3 Calculation of mass transfer rate for alkali elution

According to a batch test conducted by Tamaki et al. [23], the mass transfer rate of the alkali elution from slag into seawater was given by Eq. (3) without dependency on OH^- content in the bulk seawater because the saturated OH^- content on the slag surface was significantly larger than OH^- content in the bulk seawater and the driving force, ($[OH^-]_e$ - $[OH^-]$), of the mass transfer rate almost became $[OH^-]_e$.

$$\frac{Vd([OH^-])}{dt} = ka(t)[OH^-]_e \quad (3)$$

Here, V is the seawater volume (m^3) with 0.15 m high, 0.12 m wide and (0.235 + 0.34) m long as shown in Fig. 2, t is the time (s), k is the mass transfer coefficient (m/s) on the basis of OH^- content, a(t) is the total slag surface area contributing to alkali elution as a function of t (m^2), $ka(t)$ is the capacity coefficient of mass transfer (m^3/s), and $[OH^-]_e$ and $[OH^-]$ are the saturated OH^{-1} content (kmol/m^3) on the slag surface and bulk one in the seawater, respectively. $[OH^-]_e$ was calculated to be $10^{-1.6}$ by the solubility product of $Ca(OH)_2$ as well as Tamaki et al. [23].

As any alkali components released from the slag-packed layer travel downstream while

diffusing, the total alkali elution rate in the steady-state flow reactor (open channel vessel) can be approximately understood by the pH values at the cross section including each point of C as Eq. (4) [23], [25].

$$\frac{d(V[\mathrm{OH}^-])}{dt}=\sum_{i=1}^{5} u_i S_i \left([\mathrm{OH}^-]_\mathrm{i} - [\mathrm{OH}^-]_0\right) \quad (4)$$

Here, S_i is the representative cross-sectional area (m^2) of measurement point expressed in Fig. 11, u_i is the seawater velocity (m/s) at each point of C expressed in Figs. 5 and 6, $[\mathrm{OH}^-]_\mathrm{i}$ is the OH^- content ($kmol/m^3$) calculated from the pH value of the measurement point i in Fig. 11 and $[\mathrm{OH}^-]_0$ is the OH^- content ($kmol/m^3$) of the point a as shown in Fig. 3. The capacity coefficient, $ka(t)$ can be calculated by Eqs. (3) and (4).

The temporal changes in $ka(t)$ for the dephosphorization slag (Slag I, II) and decarburization slag (Slag III, IV) are shown in Fig. 12 (a) and (b), respectively. The $ka(t)$ values for dephosphorization and decarburization slags decreased with an increasing time. As the k value was kept constant under the unchanged operation condition, the alkali elution rate seems to reduce due to the decreasing $a(t)$, that is, f.CaO exposed on the slag surface becomes smaller by the progress of CaO dissolution and/or the slag surface is partly covered with thin precipitation layer such as $Mg(OH)_2$and Ca_2CO_3 [29], although the precipitation is not clear in this study.

The $ka(t)$ values of the dephosphorization slag in Fig. 12 (a) were about one order smaller than

1 that of the decarburization slag in Fig. 12 (b). In spite of the different particle size, the temporal
2 $ka(t)$ change for each type of slag was approximately represented by an exponentially decreased
3 curve due to the equal total slag surface area and f. CaO content. The better prediction
4 performance for decarburization slag might be due to larger pH variation to obtain the more
5 precise data in the experiment.

6 As the k value was also proportional to $\langle u \rangle^{0.35}$ as shown by Takeuchi et al. [25], each
7 regression equation was calculated in the exponential form of Eq. (5) as Eqs. (6) and (7).

8 $$ka(t) = ba_i \exp(ct) \quad (5)$$

9 Dephosphorization slag: $ka(t) = 8.71 \times 10^{-10} \langle u \rangle^{0.35} a_i \exp(-1.11 \times 10^{-5} t)$ (6)

10 Decarburization slag: $ka(t) = 1.62 \times 10^{-8} \langle u \rangle^{0.35} a_i \exp(-9.69 \times 10^{-6} t)$ (7)

11 Here, $\langle u \rangle$ is the seawater flowrate in the unit of m/s per cross-sectional area of open channel
12 vessel. From Eqs. (5) – (7), k and $a(t)$ values for dephosphorization slag are $8.71 \times 10^{-10} \langle u \rangle^{0.35}$
13 and $a_i \exp(-1.11 \times 10^{-5} t)$, respectively, whereas those for decarburization slag are $1.62 \times$
14 $10^{-8} \langle u \rangle^{0.35}$ and $a_i \exp(-9.69 \times 10^{-6} t)$, respectively.

15

16 3.4 pH change simulation with time

The temporal change in $ka(t)$ was obtained from Section 3.3. Under the assumption that the open channel vessel in this study is a mixed flow reactor, the mass balance of [OH^-] is given by the following equation [32].

$$Q[\mathrm{OH^-}]_{\mathrm{SW}} - Q[\mathrm{OH^-}] + ka[\mathrm{OH^-}]_{\mathrm{e}} = \frac{Vd[\mathrm{OH^-}]}{dt} \quad (8)$$

Here, Q is the seawater flow rate (m^3/s), $[OH^-]_{SW}$ is the OH^- content ($kmol/m^3$) in seawater. As for the left-hand side, the first term, $Q[\mathrm{OH^-}]_{\mathrm{SW}}$, is the OH^- inflow rate (kmol/s) in the open channel vessel, the second term, $Q[\mathrm{OH^-}]$, is the OH^- outflow rate (kmol/s), and the third term, $ka[\mathrm{OH^-}]_e$, is OH^- dissolution rate (kmol/s) from slag into the seawater of the open channel vessel. The term, $\frac{Vd[\mathrm{OH^-}]}{dt}$, on the right-hand side is the OH^- accumulated rate (kmol/s) in the open channel vessel. In Eq. (8), the open channel vessel flow was described as a lumped parameter system and the difference of the slag layer length and thickness in the vessel was not considered.

Substituting Eq. (5) into Eq. (8), a first-order ordinary differential equation, Eq. (8), can be solved as Eq. (10) under the initial condition of Eq. (9).

$$[\mathrm{OH^-}] = [\mathrm{OH^-}]_{\mathrm{SW}} \text{ at } t = 0 \quad (9)$$

$$[\mathrm{OH^-}] = \exp(-\frac{t}{\tau}) \times \left\{[\mathrm{OH^-}]_{\mathrm{SW}} \exp\left(-\frac{t}{\tau}\right) + \frac{ab\tau[\mathrm{OH^-}]_{\mathrm{e}}}{V(c\tau+1)} \exp\left(\left(\frac{c\tau+1}{\tau}\right)t\right) - \frac{ab\tau[\mathrm{OH^-}]_{\mathrm{e}}}{V(c\tau+1)}\right\} \quad (10)$$

First, substituting Eq. (6) or Eq. (7) into Eq. (10), the temporal change of [OH^-] was calculated. The calculated pH changes with time were compared with the experimental ones for dephosphorization and decarburization slags as shown in Fig. 13 (a) and (b), respectively. The slag conditions were shown in Table 1 and the pH values in seawater were kept at 7.90 for the calculation of dephosphorization slag and 8.19 for that of decarburization slag, respectively. The figures showed that the calculated curve for dephosphorization slag agreed well the experimental plots except at the initial stage and that for decarburization slag also had an approximately similar tendency although the data varied widely.

The calculated pH changes with time for dephosphorization and decarburization slags are shown in Figs. 14 and 15, respectively, when the slag surface area is changed as a parameter. The standard slag surface area, $a_{exp.}$, was 0.80 m^2 for dephosphorization slag and 1.07 m^2 for decarburization slag. The initial and inflow seawater pH values were kept 8.20. From both figures, the enhancement in slag surface area raised the maximum pH value and lengthened the time to converge to the seawater pH. However, even the decarburization slag with the larger free CaO content, the maximum pH value was 8.49 for $a/a_{exp.}$=5.0 ($a_{exp.}$ =1.07 m^2) and the pH increase for the seawater pH became about 0.3. The pH value was almost equal to that of the seawater in about 6 days. In the case of dephosphorization slag, the maximum pH value was

8.22 for $a/a_{exp.}$=5.0 and the pH increase became less than 0.02.

Figure 15 shows the calculated results of the temporal change in pH when the seawater flow rate Q (m^3/s) is varied as a parameter. The seawater pH value was kept 8.20 as well as Fig. 14 and the standard seawater flow rate, $Q_{exp.}$, was 1.3 m^3/h. The pH value increased with the decrease in the seawater flow rate. For example, the pH value for the decarburization slag rose up to around 8.46 for $Q/Q_{Exp.}$=0.1. On the other hand, the pH increase for the dephosphorization slag was only about 0.02. When the seawater flowed on the slag box as seen in Fig. 1 (a) [23,25], the pH value on the downstream side increased with the increasing open channel flow rate due to $k \propto <u>^{0.35}$ as expressed in Eqs. (6) and (7). However, in this simulation, the alkali elution increased with the decreasing seawater flow rate in the system where the seawater passed through the interval between slag particles packed in the open channel vessel.

The alkali elution model from steelmaking slag to seawater based on the experimental result is considered to be able to represent the pH change for the packed layer of steelmaking slag. Especially, the pH value simulation for the dephosphorization slag suggested that the alkali elution to increase the seawater pH value to a higher level did not occur in the ocean area. In the next stage, the alkali elution model which takes into account the difference at each position is required to simulate the alkali elution behavior in the large-sized space.

4. Conclusions

The alkali elution behavior of steelmaking slag into seawater was kinetically investigated and simulated for continuous flow under the condition that slag was packed in an open channel vessel using decarburization and dephosphorization slag.

1) The seawater velocity in the packed bed of slag became significantly smaller than that without packed slag.

2) The alkali elution rate of decarburization slag was larger than that of dephosphorization slag due to larger free CaO content. The pH value for dephosphorization slag was almost the same as the seawater pH in 3-4 days, while that for decarburization slag was stabilized after 3 days in spite of the pH value slightly larger than seawater.

3) The capacity coefficients of alkali elution for dephosphorization and decarburization slags decreased together in an exponential manner with time. The values of dephosphorization slag remained at one order lower level compared with those of decarburization slag.

4) Based on a regression equation on the mass transfer coefficient with time, the alkali elution behavior in an open channel flow with a packed bed of slag was simulated and calculated

1 results agreed well with experimental ones. The temporal pH change was predicted by
2 changing slag surface area or seawater flow rate as a parameter. The simulation of pH value
3 for dephosphorization slag suggested that the alkali elution to increase the seawater pH
4 value to a higher level did not occur in the ocean area.

5

6 Acknowledgements

7 This study was carried out under collaboration with Nippon Slag Association and
8 implemented with the corporation of Ushimado Marine Institute, Okayama University.

9

10 References

11 1. Nakamura Y, Taniguchi A, Okada S, Tokuda M (1998) Positive growth of phytoplankton
12 under conditions enriched with steel-making slag solution. ISIJ Int 38(4):390-398

13 2. Futatsuka T, Shitogiden K, Miki T, Nagasaka T, Hino M (2004) Dissolution behavior of
14 nutrition elements from steelmaking slag into seawater. ISIJ Int 44 (4):753-761

15 3. Tanaka M, Hirata J, Nakamoto D, Terada I, Ryumae I, Takahashi M, Oikawa T, Takahashi

K, Aimoto M (2014) Dissolution behavior of silicic acid from steelmaking slag to seawater. Tetsu-to-Hagané 100(7):919-923

4. Liu D, Yamamoto M (2014) Influence of seawater temperature and organic matter on iron elution from a mixture of steelmaking slag and composts. Tetsu-to-Hagané 100(8):1043

5. Yamamoto M, Fukushima M, Liu D (2011) Effect of humic substances on iron elution in the method of restoration of seaweed beds with steelmaking slag. Tetsu-to-Hagané 97(3):159-164

6. Zhang X, Matsuura H, Tsukihashi F (2012) Dissolution mechanism of various elements into seawater for recycling of steelmaking slag. ISIJ Int 52(5):928-933

7. Zhang X, Matsuura H, Tsukihashi F (2014) Influence of gluconic acid on dissolution of Si, P and Fe from steelmaking slag with different composition into seawater. ISIJ Int 54(6):1443-1449

8. Zhang X, Matsuura H, Tsukihashi F (2015) Enhancement of the dissolution of nutrient elements from steelmaking slag into seawater by gluconic acid. J Sustain Metall 1(2):134-143

9. Zhang X, Matsuura H, Tsukihashi F (2016) Dissolution mechanism of steelmaking

slag-dreged soil mixture into seawater. J Sustain Metall 2(2):123-132

10. Kato T, Kosugi C, Kiso E, Torii K (2015) Application of steelmaking slag to marine forest restoration. Nippon steel & Sumitomo metal technical report 109:79-84

11. Yamamoto M, Minami K, Liu D (2017) Characteristics of organic matter mixed with steelmaking slag for accelerating iron elution in seaweed bed restoration. Kagaku Kogaku Ronbunshu 43(4): 245-251

12. Hayashi A, Watanabe T, Kaneko R, Takano A, Takahashi K, Miyata Y, Matsuo S, Yamamoto T, Inoue R, Ariyama T (2012) Decrease of sulfide in enclosed coastal sea by using steelmaking slag. Tetsuto-Hagané 98 (5):207-214

13. Hayashi A, Asaoka S, Watanabe T, Kaneko R, Takano A, Takahashi K, Miyata Y, Matsuo S, Kim K, Inoue R, Ariyama T (2012) Mechanism of suppression of sulfide ion seawater using steelmaking slag. Tetsu-to-Hagané 98(11):618-625

14. Miyata Y, Hayashi A, Kuwayama M, Yamamoto T, Urabe N (2014) Reduction test of hydrogen sulfide in the silty sediment of the Fukuyama inner harbor using steelmaking slag. Tetsu-to-Hagané 100 (3):421-428

15. Miyata Y, Hayashi A, Kuwayama M, Yamamoto T, Tanishiki K, Urabe N (2014) A field

1 experiment of sulfide reduction in silty sediment using steelmaking slag. Tetsu-to-Hagané
2 100 (11):1426-1432

3 16. Kiso E, Tsujii M, Ito K, Nakagawa M, Gomyo M, Nagatome K (2008) Method of dredged
4 soil improvement by mixing with converter steel-making slag. J Civil Eng Ocean
5 24(7):327-332

6 17. Takeda M, Gomyo M, Nagatome T, Tsujii M, Kiso E, Nakagawa M (2008) Field
7 experiments on dreged soil improvement by continuously mixing with converter
8 steelmaking slag. J Civil Eng Ocean 24(7):351-356

9 18. Kanayama S, Souma A, Tanaka Y, Tsujii M, Kiso E, Nakagawa M (2008) Prediction of
10 influence on pH by utilization of mixture of dredged soil and converter steel-making slag
11 for coastal environment improvement works. J Civil Eng Ocean 24(7):333-338

12 19. Hoffert M, Wey Y C, Callegari A J, Broecker W S (1979) Atmospheric response to
13 deep-sea injections of fossil-fuel carbon dioxide. Climate Change 2(1):53-68

14 20. Sohma S, Kakio T, Sekiguchi Y (2005) Introduction of the global ocean ecosystem model
15 “DONGURI” and its implementation to investigate the biochemical effects on global

warming. Proc. 7th international conference on greenhouse gas control technologies, IEA (International Energy Agency), Paris, pp.2389-2393

21. Sakanakura H, Takahashi K, Mizutani, S (2017) Tentative test method for elution pH of steel slag applied for marine construction. Bulletin ISIJ, 22(1):36-40

22. The Japan Iron and Steel Federation (2008) Tenrokei Steelmaking Slag Kaiikiriyono Tebiki (Steelmaking Slag; a Guide for Usage in the Ocean Area), JISF, Tokyo

23. Tamaki H, Uddin M A, Kato Y, Takahashi K (2013) Alkali elution behavior of steelmaking slag into seawater by batch test. Tetsu-to-Hagané 99 (11):676-682

24. Takeuchi G, Uddin M A, Kato Y, Takahashi K (2015) Alkali elution behavior of steelmaking slag into seawater by continuous stirred tank reactor. ISIJ Int. 55(10):2252-2257

25. Takeuchi G, Uddin M A, Kato Y, Kiso E, Takahashi K (2016) Mutual effect of steelmaking slag layer depth and diameter on alkali elution rate in open channel vessel with straighten seawater flow. J Sustain Metall 3(3):459-468

26. Miyazaki T, Sakanakura H, Mizutani S, Takahashi K, Kiso E, Hirai N, Takeda M, Kurahara Y (2013) Experimental study on alkali diffusion behavior from steel slag products in steady

seawater flow. J Civil Eng B3(Ocean) 69(2):I_1142-I_1147

27. Kanayama S, Sakanakura H, Mizutani S, Kato Y, Takahashi K, Kiso E, Hirai N, Miyazaki T (2013) Study on the elution of alkalinity from steel-making slag piled in seawater. J Civil Eng B3(Ocean) 69(2):I_1152-I_1157

28. Takahashi K, Kanayama S, Sakanakura H, Mizutani S, Kiso E, Tsuda M (2015) Alkaline elution behavior of steelmaking slag in ocean construction area and its calculation simulation. J Civil Eng B3(Ocean) 71(2):I_1077-I_1082

29. Matsuda Y, Tanaka R, Okuno T, Uddin M A, Kato Y, Takahashi K, Kiso E (2019) Long-term alkali elution behavior from steelmaking slag into seawater by an open channel vessel. Tetsu-to-Hagané 106(4):471-478

30. Fukushima S (2007) Mean currents near the deep sea floor in the sea of Japan. Technical Bulletin on Hydrography and Oceangraphy 25:122-126

31. The comprehensive water quality survey in the Seto Inland Sea: (Nov. 29. 2019) http://www.pa.cgr.mlit.go.jp/chiki/suishitu/index.html

32. Levenspiel O (1999) Chemical reaction engineering. 3rd edn. John Wiley & Sons, Hoboken

1 Caption list

1 Fig. 11 Representative area of sampling points of C (unit of figure: 10^{-2} m)

2 Fig. 12 Temporal change in $ka(t)$ value and its regression curve

3 Fig. 13 Comparison between calculated and experimental pH values

4 Fig. 14 Effect of slag surface area on calculated pH change with time

5 Fig 15 Effect of seawater flow rate on calculated pH change with time

6

7

8

Table 1 Slag features used for the experiment

	Origin	Blending of Al_2O_3 balls	Mass of slag, w (kg)	Apparent density, ρ (kg/m^3)	Diameter range, d (10^{-2}m)	Mean diameter, $<d>$ (10^{-2}m)	Slag surface Area, a (m^2)	Packing ratio of slag (%)
Slag Ⅰ	Dephosphorization	Yes	4.30	$1.79x10^3$	0.95-1.32	1.32	1.08	56.0
Slag Ⅱ	Dephosphorization	No	6.44	$1.79x10^3$	1.32-2.65	2.00	1.08	52.3
Slag Ⅲ	Decarburization	Yes	6.54	$3.18x10^3$	0.95-1.32	1.15	1.07	53.2
Slag Ⅳ	Decarburization	No	11.36	$3.14x10^3$	1.32-2.65	2.02	1.07	52.4

Table 2 Chemical composition of slags used for the experiment (unit: mass%)

	CaO	SiO_2	Al_2O_3	MgO	T.Fe	f.CaO	P_2O_5
Dephosphorization	27.3	31.4	3.9	4.5	22.5	0.08	1.3
Decarburization	40.7	14.0	3.2	6.2	19.5	3.29	2.3

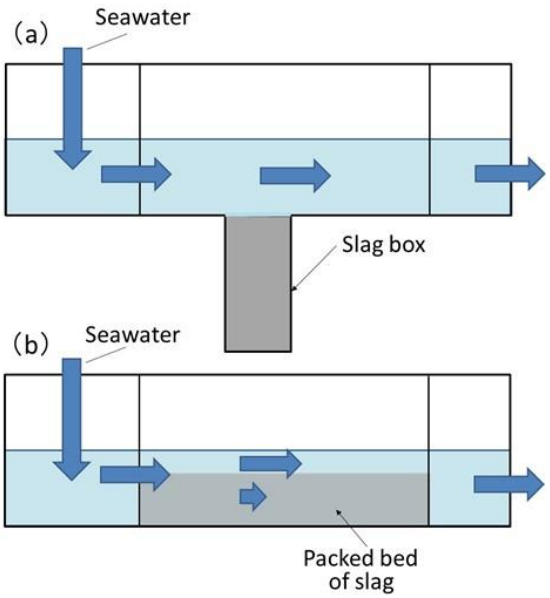

Fig. 1 Schematic diagram of packed slag position in open channel vessel.

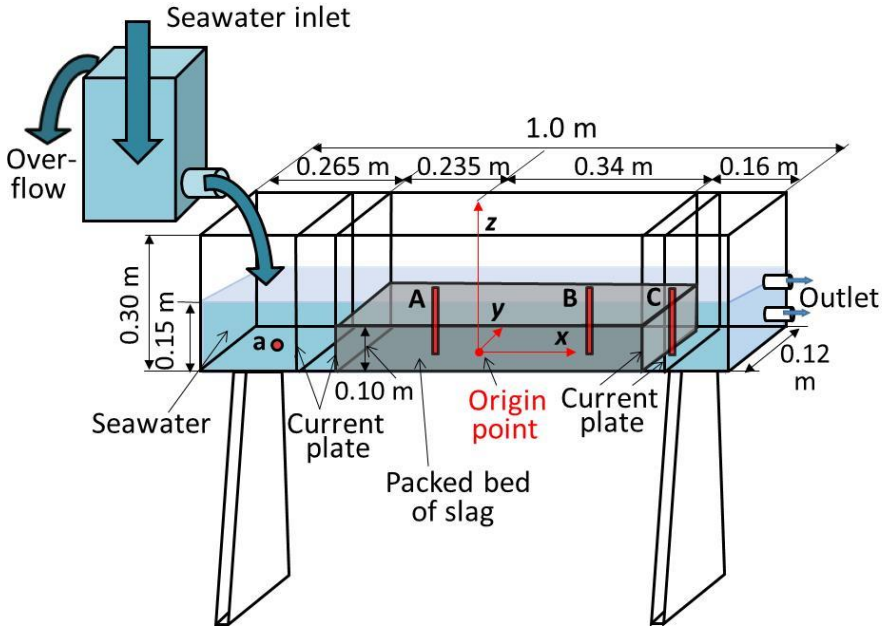

Fig. 2 Schematic diagram of experimental apparatus, packed slag position and seawater sampling sites

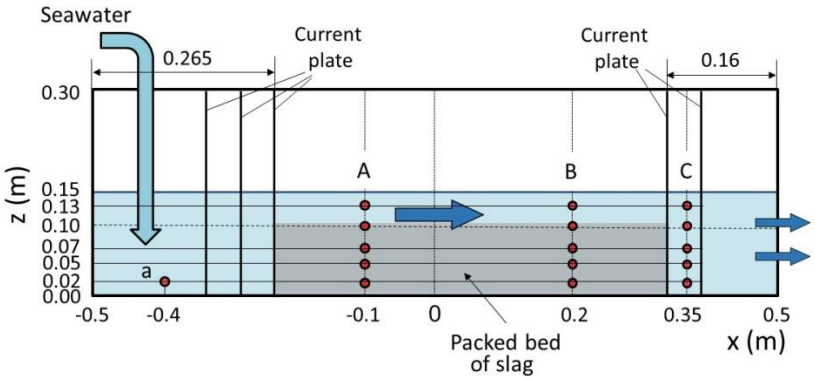

Fig. 3 Schematic diagram of sampling positions in the open channel vessel

Fig. 4 Slag samples used for the experiment

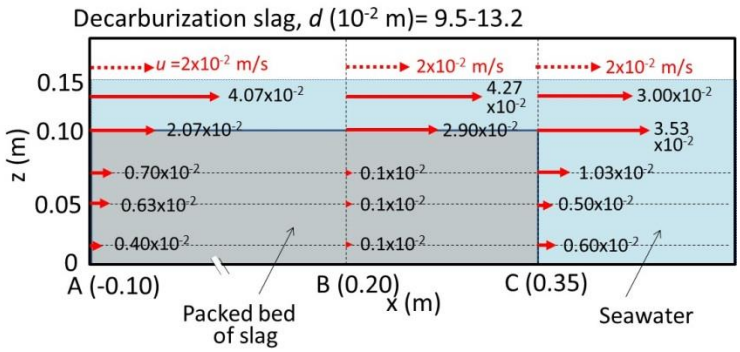

Fig. 5 x-directional velocity of seawater under slag diameter of 9.5 – 13.2 mm

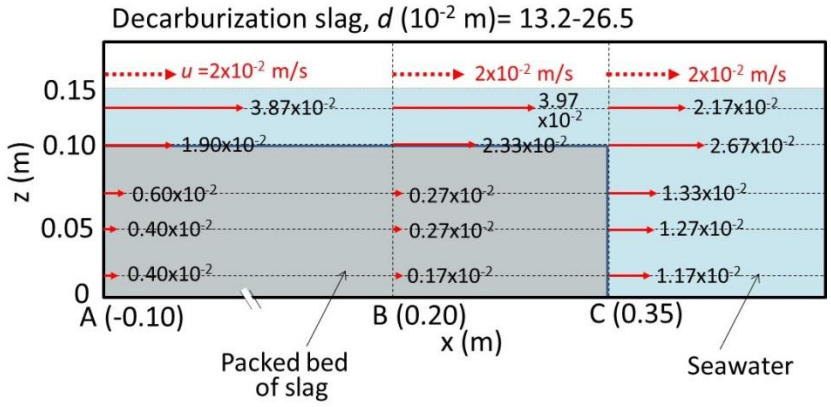

Fig. 6 x-directional velocity of seawater under slag diameter of 13.2 – 26.5 mm

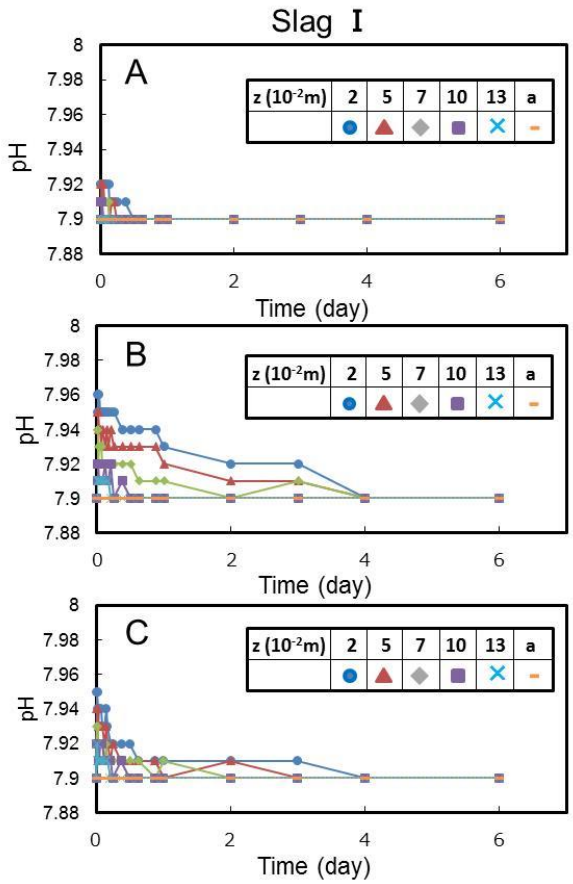

Fig. 7 Temporal change in pH distribution of dephosphorization slag (Slag I)

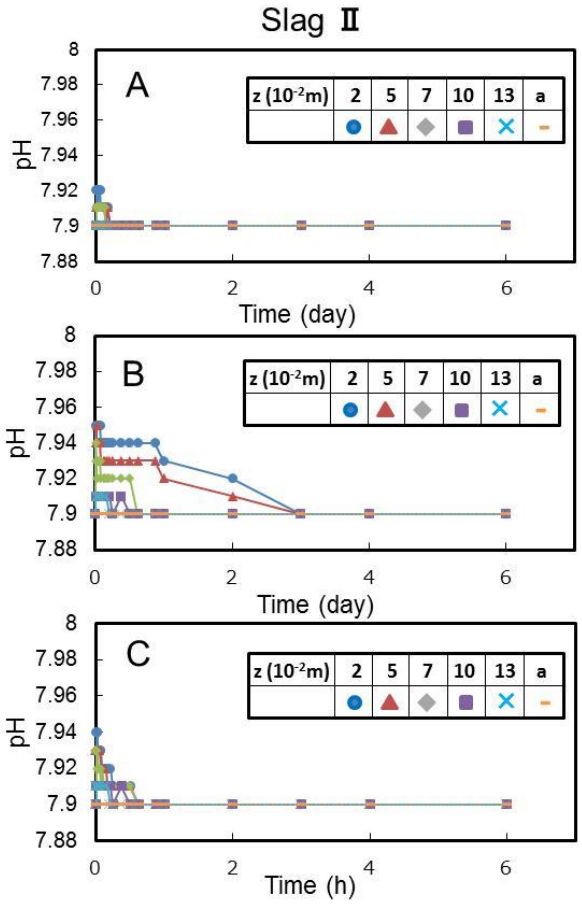

Fig. 8 Temporal change in pH distribution of dephosphorization slag (Slag II)

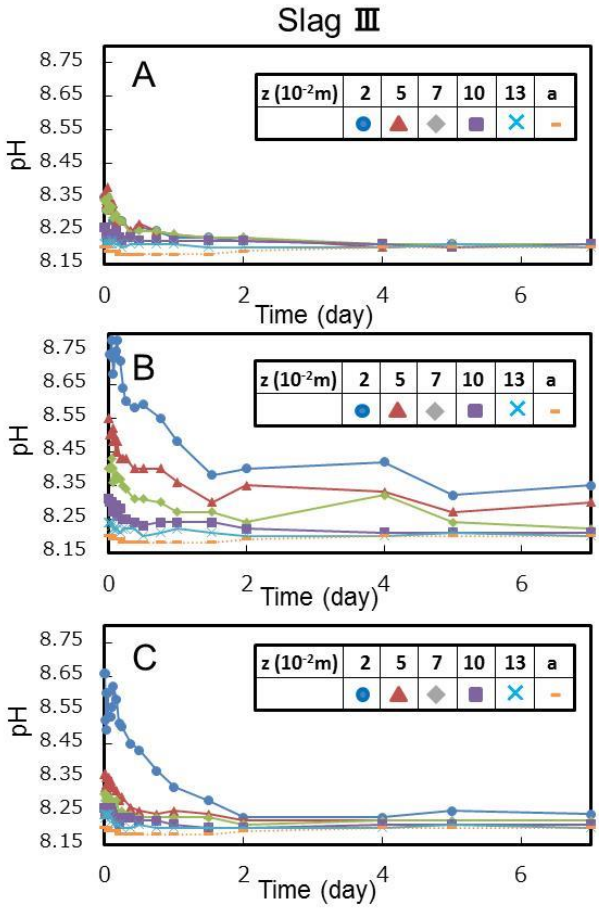

Fig. 9 Temporal change in pH distribution of decarburization slag (Slag III)

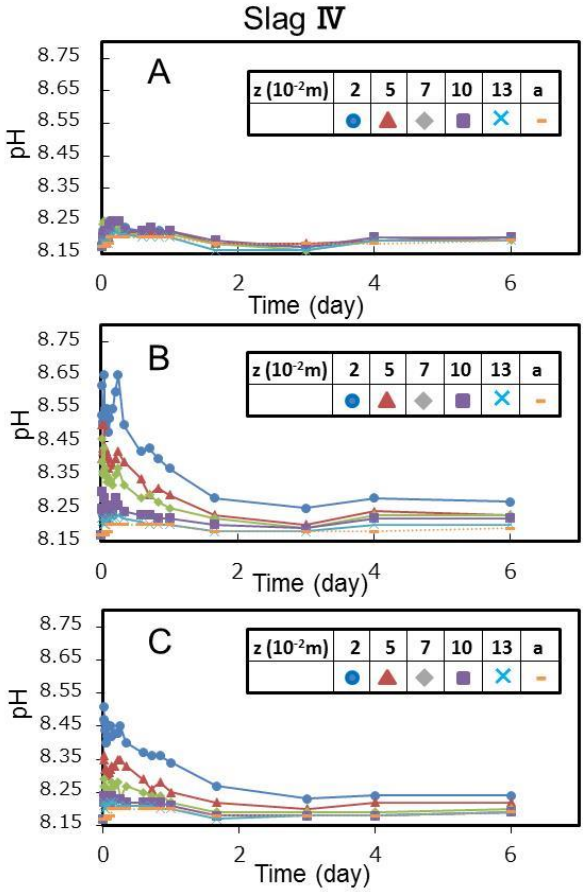

Fig. 10 Temporal change in pH distribution of decarburization slag (Slag IV)

1

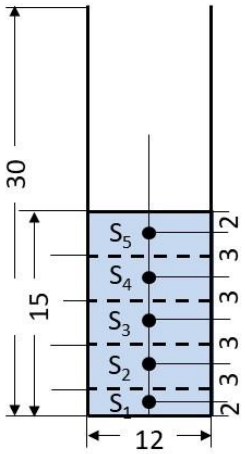

2

3

4 Fig. 11 Representative area of sampling points of C (unit of figure: 10^{-2} m)

5

6

7

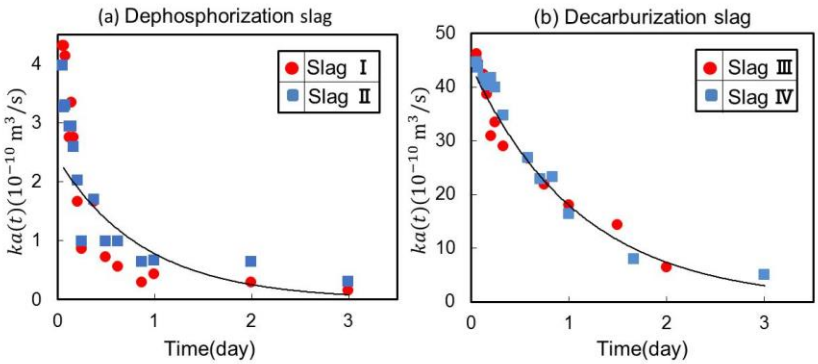

Fig. 12 Temporal change in *ka(t)* value and its regression curve

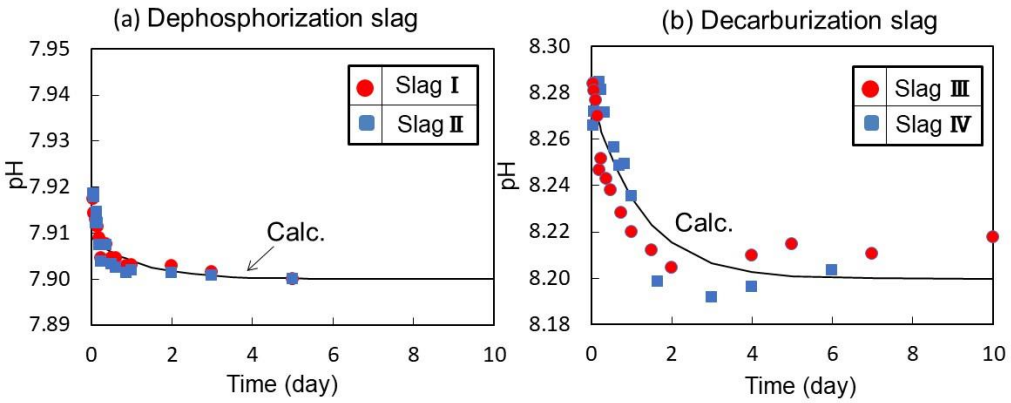

Fig. 13 Comparison between calculated and experimental pH values

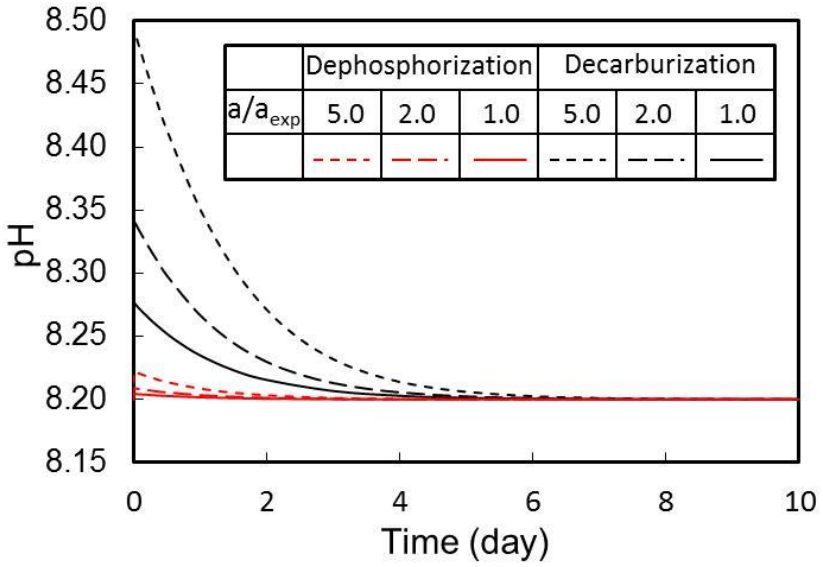

Fig. 14 Effect of slag surface area on calculated pH change with time

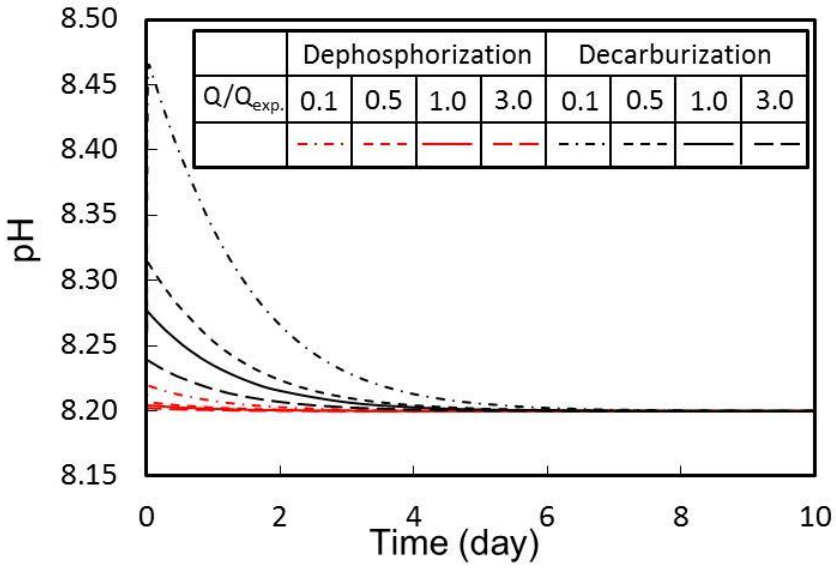

Fig 15 Effect of seawater flow rate on calculated pH change with time